

## Construction of Reference Data for Tissue Characterization of Arterial Wall Based on Elasticity Images

Jun INAGAKI, Hideyuki HASEGAWA\*, Hiroshi KANAI, Masataka ICHIKI<sup>1</sup> and Fumiaki TEZUKA<sup>2</sup>

Graduate School of Engineering, Tohoku University, Sendai 980-8579, Japan

<sup>1</sup>Sendai Hospital of East Railway Company, Sendai 983-8520, Japan

<sup>2</sup>Sendai Medical Center, Sendai 980-0022, Japan

(Received November 12, 2004; accepted February 13, 2005; published June 24, 2005)

Previously, we developed the *phased tracking method* [H. Kanai *et al.*: IEEE Trans. Ultrason. Ferroelectr. Freq. Control **43** (1996) 791] for measuring the minute change in thickness during one heartbeat and the elasticity of the arterial wall. By comparing pathological images with elasticity images measured with ultrasound, elasticity distributions for respective tissues in the arterial wall were determined. We have already measured the elasticity distributions for lipids and fibrous tissues (mixtures of smooth-muscle and collagen fiber) [H. Kanai *et al.*: Circulation **107** (2003) 3018]. In this study, elasticity distributions were measured for blood clots and calcified tissues. We discuss whether these elasticity distributions, which were measured *in vitro*, can be used as reference data for classifying cross-sectional elasticity images measured *in vivo* into respective tissues. In addition to the measurement of elasticity distributions, correlations between collagen content and elasticity were investigated with respect to fibrous tissue to estimate the collagen and smooth-muscle content based on elasticity. Collagen and smooth-muscle content may be important factors in determining the stability of the fibrous cap of atherosclerotic plaque. Therefore, correlations between elasticity and elements of the tissue in the arterial wall may provide useful information for the noninvasive diagnosis of plaque vulnerability. [DOI: 10.1143/JJAP.44.4593]

KEYWORDS: elasticity image, elasticity distribution, tissue characterization, atherosclerosis, collagen content

### 1. Introduction

Cerebral infarction and myocardial infarction are terminal symptoms of atherosclerosis. Therefore, it is important to diagnose atherosclerosis in an early stage. The rupturing of atherosclerotic plaque is probably the most important factor underlying the sudden outbreak of acute coronary syndrome.<sup>1)</sup> Direct characterization of the composition and vulnerability of atherosclerotic plaque may offer insight into the mechanism of plaque regression and progression.<sup>2,3)</sup> The elasticity of the arterial wall is largely affected by changes in composition due to the development of atherosclerosis.<sup>4)</sup> Therefore, the measurement of elasticity has the potential for arterial wall tissue characterization. For assessment of elasticity, we developed a method using transcutaneous ultrasound for measuring the minute changes in the thickness of the arterial wall during a heartbeat.<sup>5–10)</sup> In this paper, the reference data on elasticity distributions for respective tissues are presented to classify arterial tissues based on the elasticity images measured *in vivo*. From *in vitro* experiments using excised human femoral arteries, the relationship between tissue components in the arterial wall and the elasticity was investigated by comparing the elasticity images measured using ultrasound with corresponding pathological images. From *in vitro* experimental results, (1) elasticity distributions of blood clots and calcified tissues were determined in addition to those of lipids and fibrous tissues,<sup>10)</sup> and (2) the correlation between the collagen content and elasticity was investigated to noninvasively estimate collagen and smooth-muscle content in fibrous tissues based on elasticity.

### 2. Methods

#### 2.1 Elasticity estimation of arterial wall<sup>5,10)</sup>

An ultrasonic beam was sequentially scanned through  $M$

positions using a linear ultrasonic probe at 7.5 MHz with conventional ultrasound diagnostic equipment (Toshiba SSH-140A), and multiple ( $N_m + 1$ ) points were preset from the luminal surface to the adventitia along the  $m$ -th ultrasonic beam ( $m = 1, \dots, M$ ) with constant intervals of  $h_0 = 375 \mu\text{m}$  at time  $t_0$  just before the ejection period. By dividing the arterial wall into multiple layers, we defined the  $n$ -th layer ( $n = 1, \dots, N_m$ ) as being between two succeeding points,  $n$  and  $n + 1$ , along each beam. To measure the change in thickness of each of the  $N_m$  layers, the instantaneous depth  $x_{m,n}(t)$  of the  $n$ -th point along the  $m$ -th beam was simultaneously tracked by applying the *phased tracking method*<sup>5,6)</sup> to the received ultrasound. The minute decrease of several tens of micrometers in wall thickness of the  $n$ -th layer resulting from the arrival of the pressure wave at the beginning of the ejection period was determined by  $\Delta h_{m,n}(t) = x_{m,n+1}(t) - x_{m,n}(t)$ .

In the *phased tracking method*, used to calculate the auto correlation function between the quadrature demodulated signals of successively received echoes, minute phase changes of about 0.4 degrees caused by movement of the  $n$ -th point during the pulse transmission interval  $\Delta T$  ( $= 200 \mu\text{s}$ ) can be accurately determined by introducing a constraint, namely, that their waveforms are identical but their phase values change.<sup>5,6)</sup> The lowest value of the change in thickness was validated as being about  $0.5 \mu\text{m}$  by expanding a rubber plate in a water tank.<sup>7)</sup> Such a minute change in thickness cannot be measured in water by any other method. This method has already been applied with sufficient reproducibility to the *in vivo* detection of regional instantaneous displacements and changes in thickness in the carotid arteries.<sup>8)</sup>

From the ratio of the maximum decrease in thickness during one heartbeat,  $\Delta h_{m,n,\max} = \max_t |\Delta h_{m,n}(t)|$ , to the initial thickness  $h_0$  of the  $n$ -th layer, the maximum deformation of the  $n$ -th layer was obtained by  $\Delta \varepsilon_{m,n,\max} = \Delta h_{m,n,\max}/h_0$ . Since the deformation was sufficiently small

\*E-mail address: hasegawa@us.ecei.tohoku.ac.jp

and was in the linear regime, it showed incremental strain in the radial direction. By assuming that the arterial wall is incompressible and that the blood pressure is applied normal to each layer, the elastic modulus of the  $n$ -th layer along the  $m$ -th beam,  $E_{\theta,m,n}$ , is approximately given by<sup>9)</sup>

$$E_{\theta,m,n} \approx \frac{1}{2} \left( \frac{\rho_{m,n,0}}{h_0 \cdot N_m} + \frac{N_m - n + 1}{N_m} \right) \frac{\Delta p}{|\Delta \epsilon_{m,n,\max}|}, \quad (2.1)$$

where  $\rho_{m,n,0}$  is the initial inner radius of curvature of the  $n$ -th layer along the  $m$ -th beam at a time  $t_0$ . We assumed that the pressure in the arterial wall decreases linearly with the distance from the intimal side to the adventitia and that the arterial wall is almost isotropic.<sup>11)</sup>

The regional elasticity,  $E_{\theta,m,n}$ , was estimated from the cross-sectional image. Since the reflected ultrasound was received at a sampling interval of 100 ns ( $= 75 \mu\text{m}$  along depth direction) after quadrature demodulation, we further divided each layer with a thickness of  $h_0$  ( $= 375 \mu\text{m}$ ) into 5 points, shifted the initial depth of each layer with a thickness of one fifth of  $h_0$ , and applied the above procedure to each depth. Thus,  $E_{\theta,m,n}$  was estimated at intervals of  $75 \mu\text{m}$  in the depth direction.

## 2.2 Experimental system for *in vitro* experiments

Figure 1 shows the experimental setup for *in vitro* experiments using excised human femoral arteries. The change in internal pressure was generated using an artificial heart, and the internal pressure was measured with the pressure catheter (Camino 110-4) placed in the lumen of the artery. The artery fixed in the water tank was measured with a linear probe (center frequency: 7.5 MHz).

## 2.3 Construction of elasticity distribution for each tissue

In this study, the elasticity distributions were obtained with respect to blood clots and calcified tissues. After ultrasonic elasticity measurements, the arteries were fixed in formalin. The plane scanned by ultrasound was identified by imaging a needle, which was fixed in the external surface of the posterior wall, in the B-mode image during the ultrasonic measurement.<sup>10)</sup> The pathological images of the measured planes were made with elastica-masson staining for blood clots and with hematoxylin-eosin staining for calcified tissues. By referring to the pathological images, the regions which correspond to blood clots and calcified tissues were assigned in the corresponding cross-sectional elasticity

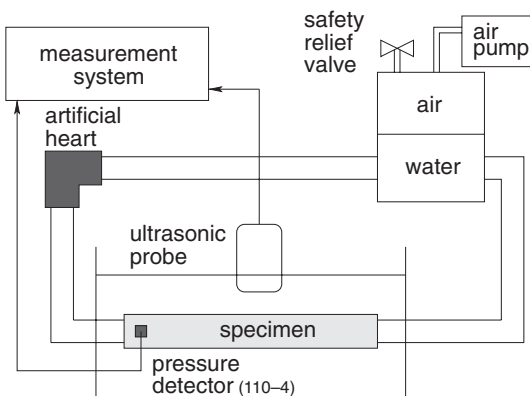


Fig. 1. Schematic diagram of the system for *in vitro* experiments.

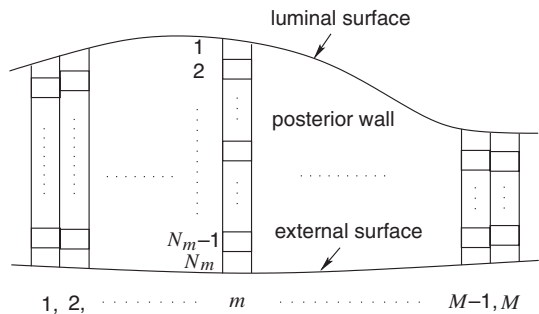


Fig. 2. Illustration of assignment of regions in a pathological image.

images. From the regions assigned for respective tissues, elasticity distributions were determined.

## 2.4 Estimation of collagen content

Fibrous tissue consists mainly of collagen fibers and smooth muscle. The correlation between the collagen content and the elasticity content was investigated with respect to fibrous tissue to noninvasively estimate the collagen and smooth muscle content based on the measured elasticity.

In the elasticity image, there are  $M$  ultrasonic beams and  $N_m$  regions along  $m$ -th beam ( $m = 1, \dots, M$ ). Therefore, in an elasticity image, there are  $\sum_{m=1}^M N_m$  regions with respective elasticity values. Each region in an elasticity image is referred as  $R_{m,n}^E$  ( $m = 1, \dots, M$ ,  $n = 1, \dots, N_m$ ). As shown in Fig. 2, each region  $R_{m,n}^E$  in the elasticity image is compared with the corresponding region  $R_{m,n}^P$  in the pathological image assigned as follows: The entire pathological image, which corresponds to the entire elasticity image, is divided into  $M$  sections in the axial direction of the artery, and each  $m$ -th section of  $M$  sections is divided into  $N_m$  regions in the radial direction. The sizes of all regions in an elasticity image are equivalent. However, actual sizes of regions assigned in the pathological image differed because of the distortion of the arterial wall due to dehydration during formalin fixation. In this paper, by assuming that the change in size due to distortion is homogeneous, each  $M$  section was divided into  $N_m$  regions of equivalent size in the radial and axial directions.

Then, the collagen content of each region  $R_{m,n}^P$  assigned in the pathological image was estimated using the Mahalanobis distance. In this paper, the composition of each region  $R_{m,n}^P$  is classified into one of four classes ( $i = 1$ : collagen, 2: smooth muscle, 3: elastin, 4: background). The mean,  $\mu_i = (\mu_r, \mu_g, \mu_b)^T$ , and covariance matrix,  $\Sigma_i$ , of RGB values were determined for each class  $i$  by manually assigning typical regions in the pathological image for each class. From the determined mean  $\mu_i$  and the covariance matrix  $\Sigma_i$ , the Mahalanobis distance  $d_i^2$  between each pixel,  $X = (x_r, x_g, x_b)^T$ , in the region  $R_{m,n}^P$  and the center of the  $i$ -th class is obtained as follows:

$$d_i^2 = (X - \mu_i)^T \sum_i^{-1} (X - \mu_i). \quad (2.2)$$

Each pixel  $X$  is classified into class  $i_{\min}$  which has the least Mahalanobis distance to  $X$ . To evaluate the collagen content in fibrous tissue, we employed two arteries mainly consisting of fibrous tissue. In other words, there are no blood clots,

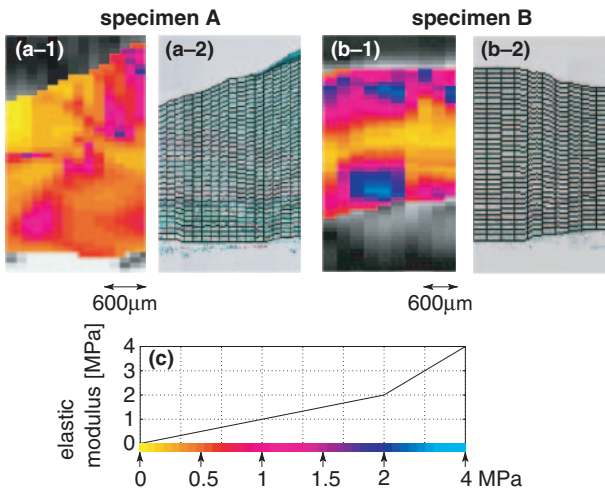


Fig. 3. Elasticity images (1) and pathological images (2) of two fibrous arteries. Divided regions,  $R_{m,n}^P$ , are shown by the black lines superimposed on the pathological images. (a) Specimen A. (b) Specimen B. (c) Colors assigned to corresponding elasticity values.

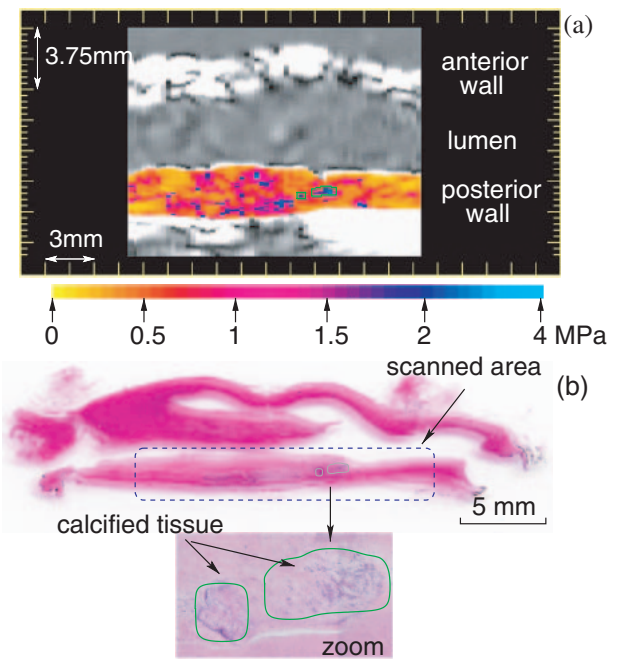


Fig. 5. (a) Elasticity image of the posterior wall of an excised human femoral artery. (b) Pathological image of the posterior wall made with hematoxylin-eosin staining.

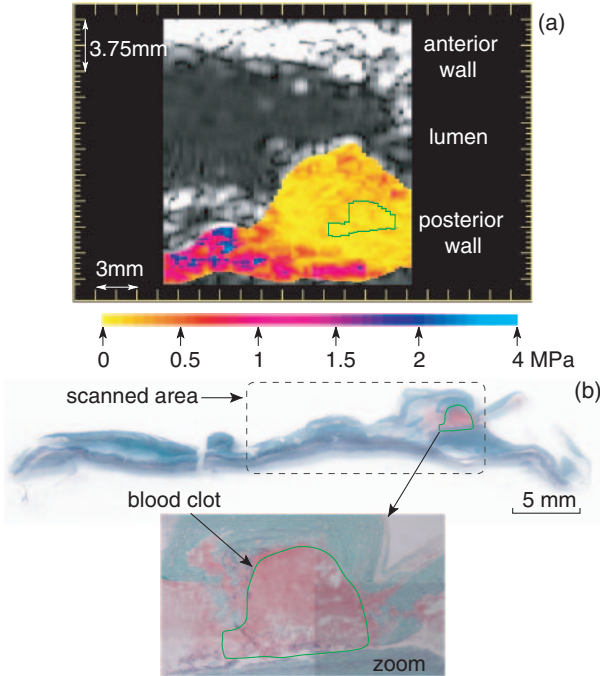


Fig. 4. (a) Elasticity image of the posterior wall of an excised human femoral artery. (b) Pathological image of the posterior wall made with elastica-masson staining.

lipids or calcified tissues in these arteries.

Figures 3(a-1) and 3(b-1) show the elasticity images of two arteries. Figures 3(a-2) and 3(b-2) show the pathological images of the corresponding sections. Black meshes show divided regions  $R_{m,n}^P$  which correspond to  $R_{m,n}^E$  in the respective elasticity images. Figure 3(c) shows the colors assigned to corresponding elasticity values.

In the process for creating the pathological image, some deformations unavoidably occur. Such deformations lead to differences in size and shape between the elasticity and pathological images. Therefore, we used a part of the arterial wall showing little difference in size and shape between the elasticity image and the pathological image.

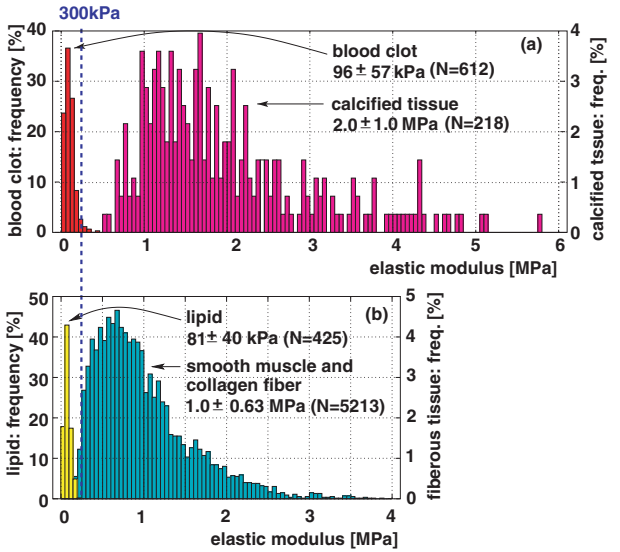


Fig. 6. (a) Elasticity distributions of blood clots and calcified tissues. (b) Elasticity distributions of lipids and fibrous tissues (mixtures of smooth muscle and collagen fibers).<sup>10</sup>

The resolution was too small to exactly correlate a region in the elasticity image to the corresponding region in the pathological image because of the deformation caused by dehydration. Therefore, we employed spatially averaged values obtained from regions with about 600 μm in the axial direction × 600 μm in the radial direction in size.

### 3. Results

#### 3.1 Construction of elasticity distribution for each tissue

Figures 4(a) and 5(a) show the elasticity images of two excised human femoral arteries. After ultrasonic measurement, the pathological images of the measured sections were made as shown in Figs. 4(b) and 5(b) with elastica-masson

staining and hematoxylin-eosin staining, respectively. From the respective pathological images, the blood clot and the calcified tissue were identified as shown by the regions surrounded by green lines in Figs. 4(b) and 5(b). The means and standard deviations with respect to elastic modulus were determined to be  $96 \pm 57$  kPa for the blood clot and  $2.0 \pm 1.0$  MPa for the calcified tissue, where the number of points assigned in the elasticity images were 612 and 278, respectively.

Figure 6 shows the elasticity distributions of the blood clot, calcified tissue, lipid, and fibrous tissue (mixture of collagen fiber and smooth-muscle).<sup>10)</sup> By comparing each elasticity distribution, great similarity was found in the elasticity distributions of lipids and blood clots. This means that the classification of these tissues based on elasticity is difficult. Moreover, the elasticity distributions of fibrous tissue and calcified tissue largely overlapped each other. However, it will be possible to classify lipids or blood clots from fibrous tissues or calcified tissues. These two groups (soft and hard tissues) may be distinguished at about 300 kPa. These results suggest that hard tissues such as fibrous tissues and calcified tissues, which contribute to the stability of plaque, and soft tissues such as lipids and blood clots, which contribute to instability, can be noninvasively differentiated based on elasticity.

### 3.2 Relationship between collagen content and elasticity

Figure 7 shows the relationship between the collagen content and the elasticity for the two fibrous arteries shown in Figs. 3(a) and 3(b). In Fig. 7, plots and vertical bars show the spatial means and standard deviations within regions about  $600 \mu\text{m} \times 600 \mu\text{m}$  in size. There are 36 points, which were calculated from 758 divided regions  $R_{m,n}^E$ . The straight line shows the regression line obtained by applying the least-squares method to the spatial means. A positive correlation between collagen content and elasticity was found.

Figures 8(a) and 8(b) show the relationship between the collagen content and the smooth-muscle content in each divided region  $R_{m,n}^P$  and each spatial averaging region of about  $600 \mu\text{m} \times 600 \mu\text{m}$ , respectively. In this estimation, regions were manually assigned twice with respect to the same pathological image to estimate both collagen and smooth-muscle content in a divided region. In the first assignment, the collagen content of each divided region  $R_{m,n}^P(1)$  was estimated. In the second assignment, the smooth-muscle content of each divided region  $R_{m,n}^P(2)$  was

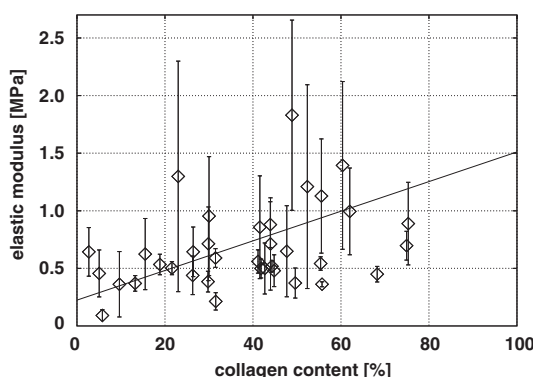


Fig. 7. Relationship between collagen content and elasticity.

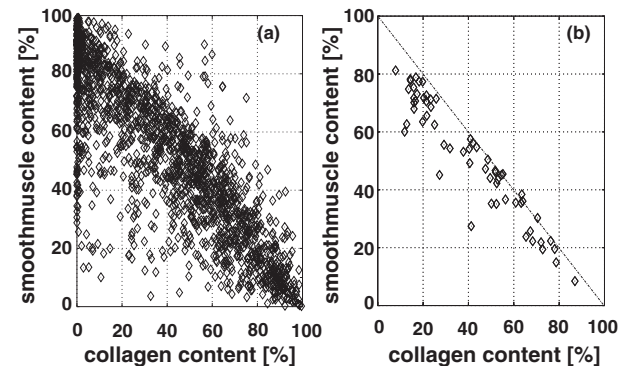


Fig. 8. Relationship between collagen content and smooth muscle content in the region with the pathological image. (a) Before spatial averaging. (b) After spatial averaging.

estimated. Then, the collagen content in  $R_{m,n}^P(1)$  v.s. the smooth-muscle content in  $R_{m,n}^P(2)$  was plotted in Fig. 8(a). There are some points for which the sum of collagen and smooth-muscle content show a value of over 100% in Fig. 8(a). This means that the sizes and positions of  $R_{m,n}^P(1)$  and  $R_{m,n}^P(2)$  were not identical. This result suggests that the size of each divided region  $R_{m,n}^P$  is too small to identify a region in the arterial wall, especially in the case of comparing the elasticity image with the pathological image, because the deformation due to dehydration also influences the values. As shown in Fig. 8(b), almost all the sums of collagen and smooth-muscle content are below 100% after spatial averaging with respect to a region  $600 \mu\text{m} \times 600 \mu\text{m}$  in size. This result suggests that the influence of region disagreement was reduced by comparing larger regions. Therefore, we also applied spatial averaging to estimate the relationship between collagen content and elasticity.

In Fig. 8(b), most sums of both contents were about 90%, which shows that fibrous arteries consist mainly of collagen and smooth muscle. By assuming that the fibrous tissue consists of only collagen and smooth muscle, we estimate the collagen and smooth muscle content of fibrous tissue based on its elastic modulus. Figures 9(a) and 9(b) show the collagen and smooth-muscle content for each elasticity value superimposed on the elasticity distribution of fibrous tissues shown in Fig. 6(b). From the correlation shown in Fig. 7, collagen and smooth-muscle content can be estimated as shown in Figs. 9(a) and 9(b) based on elasticity measured with transcutaneous ultrasound.

## 4. Conclusions

By comparing the elasticity distributions of blood clots, calcified tissues, lipids and fibrous tissues,<sup>10)</sup> it was found that arterial tissues can be classified into soft tissues (lipids or blood clots) and hard tissues (fibrous tissues or calcified tissues) from the elasticity image. These two groups were distinguished at about 300 kPa, and this threshold is important to make a rough tissue characterization based on elasticity. Furthermore, comparing collagen content and elasticity, a positive correlation was found. This result offers the potential of estimating collagen content based on elasticity, and this collagen-content estimation may contribute to noninvasive evaluations of the vulnerability of atherosclerotic plaques.

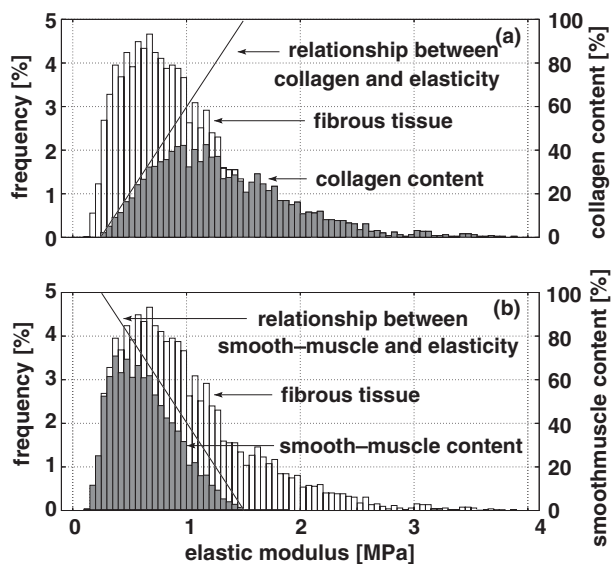


Fig. 9. Estimated (a) collagen content and (b) smooth muscle content contained in fibrous tissue superimposed on the elasticity distribution of fibrous tissue.

- 1) P. R. Moreno, E. Falk, I. F. Palacios, J. B. Newell, V. Fuster and J. T. Fallon: *Circulation* **90** (1994) 775.
- 2) H. M. Loree, R. D. Kamm, R. G. Stringfellow and R. T. Lee: *Circ. Res.* **71** (1992) 850.
- 3) E. Falk, K. Prediman, P. K. Shah and V. Fuster: *Circulation* **92** (1995) 657.
- 4) R. T. Lee, A. J. Grodzinsky, E. H. Frank, R. D. Kamm and F. J. Schoen: *Circulation* **83** (1991) 1764.
- 5) H. Kanai, M. Sato, Y. Koiwa and N. Chubachi: *IEEE Trans. UFFC* **43** (1996) 791.
- 6) H. Kanai, H. Hasegawa, N. Chubachi, Y. Koiwa and M. Tanaka: *IEEE Trans. UFFC* **44** (1997) 752.
- 7) H. Kanai, K. Sugimura, Y. Koiwa and Y. Tsukahara: *Electron. Lett.* **35** (1999) 949.
- 8) H. Kanai, Y. Koiwa and J. Zhang: *IEEE Trans. UFFC* **46** (1999) 1229.
- 9) H. Hasegawa, H. Kanai, N. Hoshimiya and Y. Koiwa: *Jpn. J. Med. Ultrason.* **31** (2004) 81.
- 10) H. Kanai, H. Hasegawa, M. Ichiki, F. Tezuka and Y. Koiwa: *Circulation* **107** (2003) 3018.
- 11) D. J. Patel, J. S. Janicki, R. N. Vaishnav and J. T. Young: *Circ. Res.* **32** (1973) 93.